PHOTONICS Research

Low phase noise K-band signal generation using polarization diverse single-soliton integrated microcombs

Alwaleed Aldhafeeri,[1,*] Hsiao-Hsuan Chin,[1] Tristan Melton,[1] Dong IL Lee,[1] Allen Chu,[1] Wenting Wang,[1] Mingbin Yu,[2,3] Patrick Guo-Qiang Lo,[2] Dim-Lee Kwong,[2] and Chee Wei Wong[1,4]

[1] *Fang Lu Mesoscopic Optics and Quantum Electronics Laboratory, University of California, Los Angeles, California 90095, USA*
[2] *Institute of Microelectronics, A*STAR, Singapore 117865, Singapore*
[3] *State Key Laboratory of Functional Materials for Informatics, Shanghai Institute of Microsystem and Information Technology, and Shanghai Industrial Technology Research Institute, Shanghai 200050, China*
[4] *e-mail: cheewei.wong@ucla.edu*
**Corresponding author: aaldhafe@ucla.edu*

Received 13 February 2024; revised 14 March 2024; accepted 20 March 2024; posted 25 March 2024 (Doc. ID 521282); published 27 May 2024

Frequency microcombs with microwave and millimeter-wave repetition rates provide a compact solution for coherent communication and information processing. The implementation of these microcombs using a CMOS-compatible platform further paves the way for large-scale photonic integration and modularity. Here, we demonstrate free-running soliton microcombs with K-band repetition rates with very low phase noise over a 4 GHz pump detuning range reaching −117 (−123) dBc/Hz at 10 kHz offset for a 19.7 (10) GHz carrier without active pump stabilization, exceeding commercial electronic microwave oscillators at frequency offsets above 40 kHz. The minimum laser noise to soliton microwave signal transduction factor observed is −73 dB. This noise performance is achieved using a hybridized dual-mode for soliton generation to achieve passive thermal stabilization and minimal soliton spectrum shift from prior Raman scattering and dispersive wave formation. We further examine the locking of the repetition rate to an external ultrastable photonic oscillator to illustrate the feasibility of phase noise suppression below the thermorefractive noise limits of microresonator frequency combs.

https://doi.org/10.1364/PRJ.521282

1. INTRODUCTION

The emergence of microresonator-based frequency combs (microcombs) has shaped the path toward miniaturized and scalable photonic devices [1–4]. In addition to their compactness, microcombs can be designed with comb spacing or free spectral ranges (FSR) from 2.6 GHz up to 1 THz [5–8] as opposed to fiber or solid-state mode-locked lasers where the comb fundamental repetition rate is often in the GHz range due to the bulk materials and cavity sizes [9–13]. Dissipative Kerr solitons (DKSs), where the temporal shape of the pulse is preserved due to achieving a balance between nonlinear gain and dispersion, can form in the microresonator [14–19]. The smooth spectrum and high coherence of the comb lines make DKS suitable for a wide variety of applications, such as optical frequency synthesis [20], optical clockworks [6], microwave generation [21,22], coherent optical communications [23], distance measurements [24,25], exoplanet searching [26], and optical coherence tomography [27].

Microwave signals derived from frequency combs feature high spectral purity because they are derived from a large division of the noise from the optical to the microwave frequencies via photodetection of the pulse train [28]. As a result, the small size, weight, and power (SWaP) and optical-to-microwave noise reduction have increased interest in microcombs, including those with low repetition rates [5,29]. Recently, DKS with microwave FSR has been demonstrated in different structures and materials such as crystalline microresonators [21,30,31], silica [32–35], silicon nitride (Si_3N_4) [7,8,14,22,36–39], and lithium niobate [40]. In particular, complementary metal–oxide semiconductor (CMOS) compatible planar integrated microresonators are of great interest because of their monolithic electronic and photonic integration capabilities. The lowest phase noise for a microwave carrier was achieved in crystalline microresonators [21,30]; however, they are not CMOS compatible for large-scale integration. Silica has demonstrated very low-noise microwave signal carriers due to their low thermal noise, but the low index of silica makes it difficult for monolithic integration, leading to the use of tapered fibers for optical coupling of the resonator [32,33]. Si_3N_4 microresonators show the most promising path toward full monolithic integration due to their integrated planar design and the simplicity of mode and dispersion engineering compared to the abovementioned materials; however, the generated microwave signals from these microresonators to date have shown higher phase noise compared to other materials [22,36].

The noise sources in the DKS-based microwave oscillators have been studied extensively [22,31,32,41–43]. The performance of these microwave oscillators still has not reached their fundamental limit given by the fundamental thermorefractive noise (TRN) of the microresonators [44,45] due to the presence of other higher noise sources such as laser phase noise transduction due to detuning dependent Raman self-frequency shift (RSFS) and soliton recoil induced by dispersive waves [31,42,46,47]. Such a phenomenon has been exploited to reduce the phase noise of the soliton repetition rate by operating on a narrow pump detuning region such that RSFS is balanced by soliton recoil where the repetition rate dependence on detuning is minimized, which is known as quiet point operation [41]. Furthermore, the use of an auxiliary mode has been demonstrated to provide passive thermal stabilization of the resonator and hence reduce the repetition rate phase noise [42,48,49]. The auxiliary mode provides a cooling effect such that the auxiliary mode pins the main resonance, which leads to fixed pump-cavity detuning. Also, it has been shown that power fluctuations within the microresonator can couple to the phase noise of the soliton repetition rate [50]. Dispersive waves induced by avoided mode crossing (AMX) [32] introduce additional spatiotemporal thermal noise to the soliton repetition rate through uncorrelated thermal fluctuations between different modes of the microresonator.

Here, we show that a soliton with a low phase noise over a large 4 GHz detuning range can be achieved by both minimizing the detuning-dependent RFSS and soliton recoil, and the use of a hybridized mode for self-thermal stabilization and a stable soliton generation. We achieve a measured single-sideband phase noise lower than −110 dBc/Hz at 10 kHz offset from the 19.69 GHz carrier over the detuning range reaching a minimum of −117 dBc/Hz (−123 dBc/Hz-scaled to 10 GHz), which is, to the best of our knowledge, the lowest phase noise achieved in free-running microwave chip-based DKS without applying any active stabilization. Furthermore, we show that active stabilization of the DKS can overcome the TRN by locking the soliton repetition rate to an external reference derived from fiber-based frequency combs, with a resulting microwave phase noise lower than the microresonator TRN.

2. RESULTS AND DISCUSSION

A. Single Soliton Generation

To generate a self-stabilized soliton microcomb, a tunable external cavity diode laser (ECDL) is amplified by an L-band erbium-doped fiber amplifier (EDFA), sent to a polarization beam splitter (PBS) to select the TM mode, and then coupled to a strongly coupled dispersion-managed paw-shaped compact Si_3N_4 microresonator with a single facet coupling loss of 3 dB resulting in ≈800 mW on-chip power. This is illustrated in Fig. 1(a). A single soliton is generated via manual forward piezoelectric laser wavelength tuning into the resonance, followed by a small backward detuning to fall into the soliton state [18,51,52]. The soliton has an existence range of several GHz due to the auxiliary mode; once the soliton is generated, it stays for hours without any active stabilization. At the output, a fiber Bragg grating (FBG) is used to filter the pump from the spectrum before amplifying the comb power to ≈20 mW. The amplified comb is subsequently sent into a fast high-power photodiode and the detected radio frequency (RF) beat is filtered by a bandpass filter and amplified to ≈7.9 dBm by a low-phase noise RF amplifier.

The free spectral range (FSR) and loaded quality factor (Q) of the fundamental TE mode are ≈19.69 GHz and ≈1.4 million, respectively. The optical spectrum of the 19.69 GHz soliton is shown in Fig. 1(c) via an optical spectrum analyzer (OSA; Yokogawa) with a 50 pm resolution. The measured local second-order dispersion near the AMX is found to be $D_2/2\pi = 30.1 \pm 4.6\,\mathrm{kHz}$ (see Appendix A). The presence of third-order dispersion leads to the formation of a dispersive wave near 1870 nm, which leads to asymmetry in the optical spectrum. Such asymmetry and the presence of an AMX signature at the pump result in the spectrum differing from a baseline sech^2 fit, as illustrated in Fig. 1(c). By using the comb lines around the pump, an example sech^2 fit is shown in orange, where there is no OSA-discernible soliton self-frequency and recoil shift from the pump.

B. Noise and Instability Characterization

Figure 2(a) shows the detected microwave signal at 19.69 GHz and phase noise characteristics in the free-running state. The detected microwave beat RF spectrum is shown in Fig. 2(b) with 1 kHz RBW. The absolute single-sideband (SSB) phase noise power spectral density of the 19.69 GHz microwave carrier is measured using a phase noise analyzer (Rohde & Schwarz FSWP26) and reaches −85 dBc/Hz at 1 kHz offset, −117 dBc/Hz at 10 kHz, and −137 dBc/Hz at 100 kHz. At higher offset frequencies, the microresonator noise is limited at −147 dBc/Hz, which is about 3 dB higher than the estimated shot noise. This higher noise floor is caused by amplified spontaneous emission (ASE) from EDFA [53].

The soliton repetition rate is expressed as

$$f_{\mathrm{rep}} = \frac{1}{2\pi}\left[D_1 + \frac{D_2}{D_1}\Omega(\Delta)\right], \qquad \textbf{(1)}$$

where $D_1/2\pi$ is the FSR and $D_2/2\pi$ is the second-order dispersion of the microresonator, $\Omega(\Delta)$ is the detuning dependent total spectrum shift due to the Raman-induced soliton self-frequency shift (SSFS) Ω_{Raman} and the dispersive-wave-induced frequency recoil of the soliton Ω_{Recoil}. Δ is the difference between the pump frequency and the cold cavity frequency. The soliton repetition rate phase noise originates from different sources. It can be seen that the contribution of the fluctuations of $\Omega(\Delta)$ to f_{rep} can be reduced by minimizing D_2 or $\Omega(\Delta)$, or both. Besides, the different contributions of soliton repetition rate noise $S^{\phi}_{f_{\mathrm{rep}}}$ can be expressed as [22,32]

$$S^{\phi}_{f_{\mathrm{rep}}} = \beta^2 S_{\delta f,p} + \frac{\alpha^2}{f^2} S_{\mathrm{RIN},p} + \gamma^2 \omega_p^2 S_{\mathrm{AMX}} + D_1^2 S_{\mathrm{TRN}} + S_Q, \qquad \textbf{(2)}$$

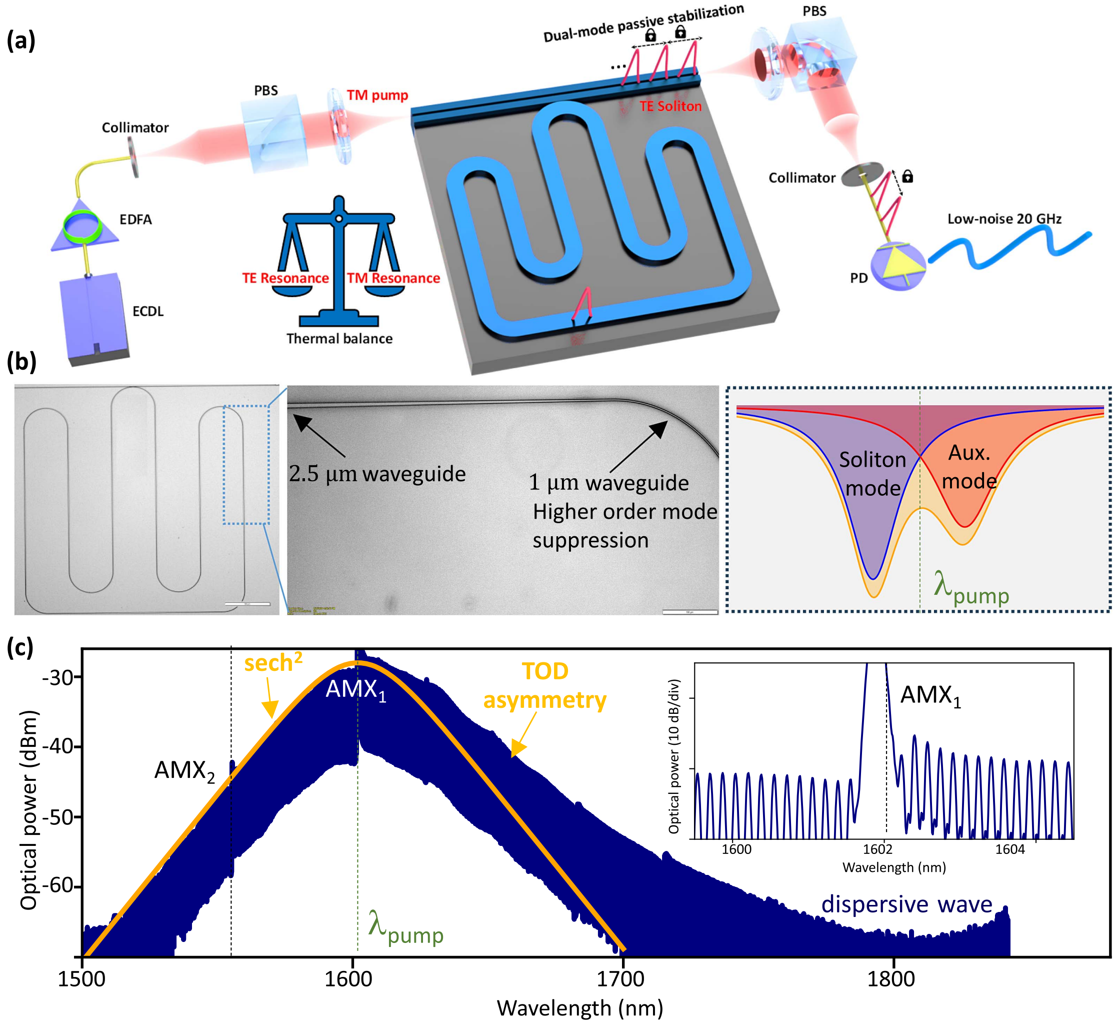

Fig. 1. (a) Illustration of the experimental setup of low noise microwave generation due to the hybridized mode using polarization diverse soliton. (b) Microscope images of the PAW resonator. Right panel illustrates the dual auxiliary (TM$_0$) and soliton mode (TE$_0$) interactions. (c) Measured optical spectrum of the polarization dissipative soliton. The spectrum does not fit a sech^2 profile due to its asymmetry. Inset: optical spectrum near the pump showing a signature of an AMX.

where $S_{\delta f,p}$ is the pump phase noise, $\beta^2 = \frac{\partial f_{\mathrm{rep}}}{\partial \delta f_p}$ is the optical-to-microwave phase transduction (PM-to-PM) coefficient of the laser noise, $S_{\mathrm{RIN},p}$ is the pump intensity noise that is related to the soliton repetition rate phase noise by applying a $1/f^2$ factor, and α^2 is the transduction factor of the intensity noise of the pump to the phase noise of soliton repetition rate through the Kerr effect [22,31,50]. S_{AMX} is the AMX-induced spatiotemporal thermal noise of the hybridized mode [32], ω_p is the frequency of the pump laser, γ^2 is the transduction factor of the spatiotemporal thermal fluctuations to the phase noise of soliton repetition rate, S_{TRN} is the thermorefractive noise of the soliton mode [44], and S_Q is the quantum jitter. First, we measure the frequency noise of our ECDL by heterodyne beating with a 1 Hz linewidth stable laser to estimate the influence of the frequency noise of our ECDL in the generated microwave signal. The noise transfer from our laser to microwave noise (PM-to-PM) transduction coefficient (β^2) is estimated at −73 dB, as shown in black in Fig. 2(a). This is evidenced by the ECDL noise features imprinted on the microwave beat note at an offset below 2 kHz as well as a slight noise bump at the 20 kHz offset. This is further verified by modulating the phase of the pump laser by a 5 kHz sinusoidal signal to act as a calibration tone in the soliton microwave beat power spectral density [31]. Compared to the best existing Si$_3$N$_4$-based low repetition rate free-running DKS [22], our PM-to-PM transduction is 18 dB lower.

The laser PM-to-PM is only 7 dB higher than the limit imposed by phase noise reduction due to the optical-to-microwave division ($20\log_{10}\frac{f_{\mathrm{pump}}}{f_{\mathrm{rep}}} = 80$ dB). In addition, we investigate the noise contribution preventing us from achieving even lower noise. The intensity fluctuation of the laser pump and EDFA is measured as the relative intensity noise (RIN), as shown in Fig. 2(c). The intensity noise of the pump transduction to the phase noise in the microresonator does not seem to be a limiting factor at any frequency offset, as shown in orange

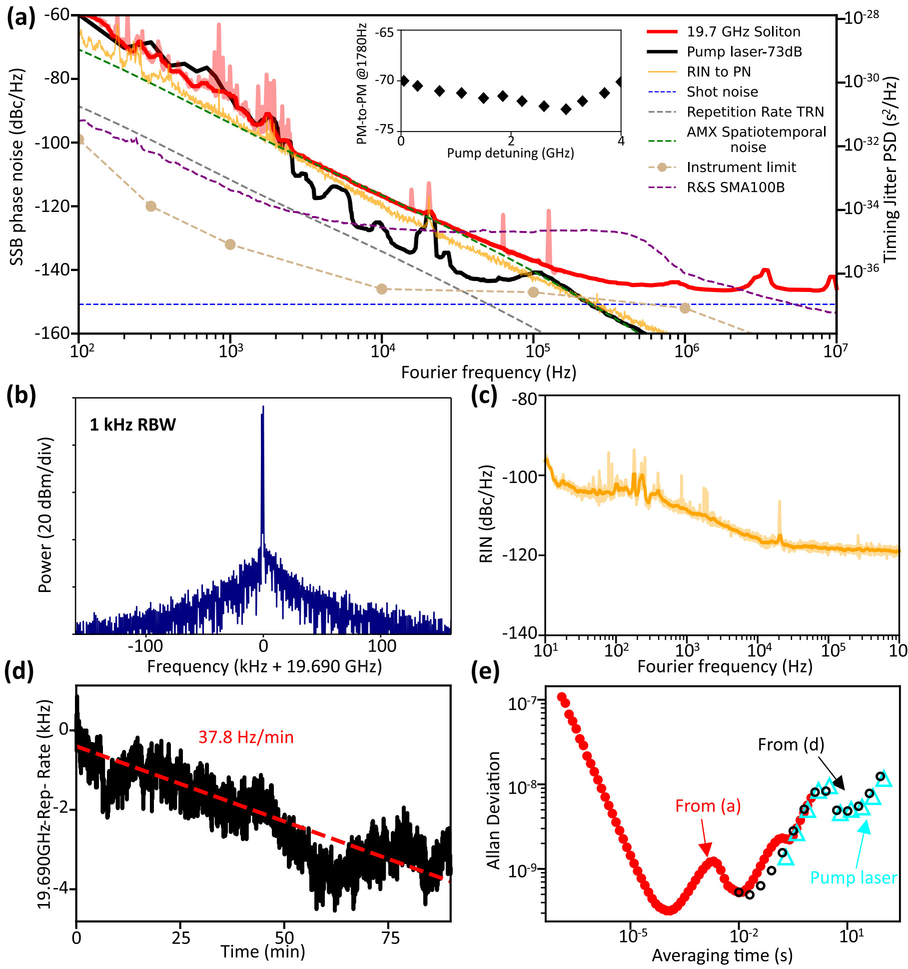

Fig. 2. Characterization of the free-running soliton repetition rate. (a) Single-sideband (SSB) phase noise was measured with the free-running microresonator. The estimated shot noise floor is −150 dBc/Hz. Pump laser phase noise transduction to repetition rate noise is shown in black. The estimated noise induced by pump intensity fluctuation is plotted in orange, which is not the noise limiting factor. The simulated AMX-induced noise originating from intermode thermorefractive noise (TRN) is illustrated in green. Repetition rate TRN is the fundamental limit of the generated microwave beat and is shown in light gray. For comparison, the noise of a Rohde & Schwarz SMA100B signal generator is illustrated in purple. The phase noise analyzer FSWP26 instrument limit is shown as the dashed light brown line. Inset: pump laser phase noise transduction at 2 kHz offset for 0 to 4 GHz detuning. (b) RF spectrum of the microwave repetition rate beat signal with a resolution bandwidth (RBW) of 1 kHz. (c) Relative intensity noise (RIN) of the pump laser and EDFA. (d) A frequency counter measurement shows the real-time trace of the repetition rate, with a long-term average drift of −37.8 Hz/ min over 85 min. (e) Repetition-rate beat Allan deviation computed from single-sideband phase noise metrology [(a) in red] and frequency counting [(d) in black].

in Fig. 2(a), where the fit represents the maximum possible noise transduction. The dominant noise at offsets higher than 2 kHz corresponds to the dispersive wave noise due to the AMX among the soliton mode, and fundamental transverse electric mode (TE_0), and the fundamental transverse magnetic mode (TM_0). The calculation of the AMX-induced spatiotemporal thermal noise fits well with the measured phase noise of the soliton at offsets higher than 2 kHz with $\gamma^2 = 58$ dB in our microcomb subsystem (see Appendix B).

In prior chip-based microresonators, similar performance relies on finding a quiet point, which is a specialized detuning where the laser frequency noise influence on the repetition rate noise is minimal due to the intricate balance between the Raman self-frequency shift and soliton recoil, as shown in Eq. (1) [41]. The existence range of such detuning is on the order of the cavity linewidth; hence, active stabilization of the pump-cavity detuning is required [31,32,41]. In our microresonator, we demonstrate that the soliton repetition rate phase noise can be reduced by minimizing Ω. Thus, no active stabilization of the pump or the resonator is used. We are able to achieve a very low phase noise operation covering more than 4 GHz detuning, as shown in Fig. 3. This is due to the effect of the hybridized mode on minimizing the thermal impact of the pump-cavity detuning [48,51]. We also compare our microresonator performance with commercially available high-performance microwave local oscillators where the phase noise of the soliton microwave beat note becomes comparable to or better than that for offset frequencies higher than 20 kHz. Table 1

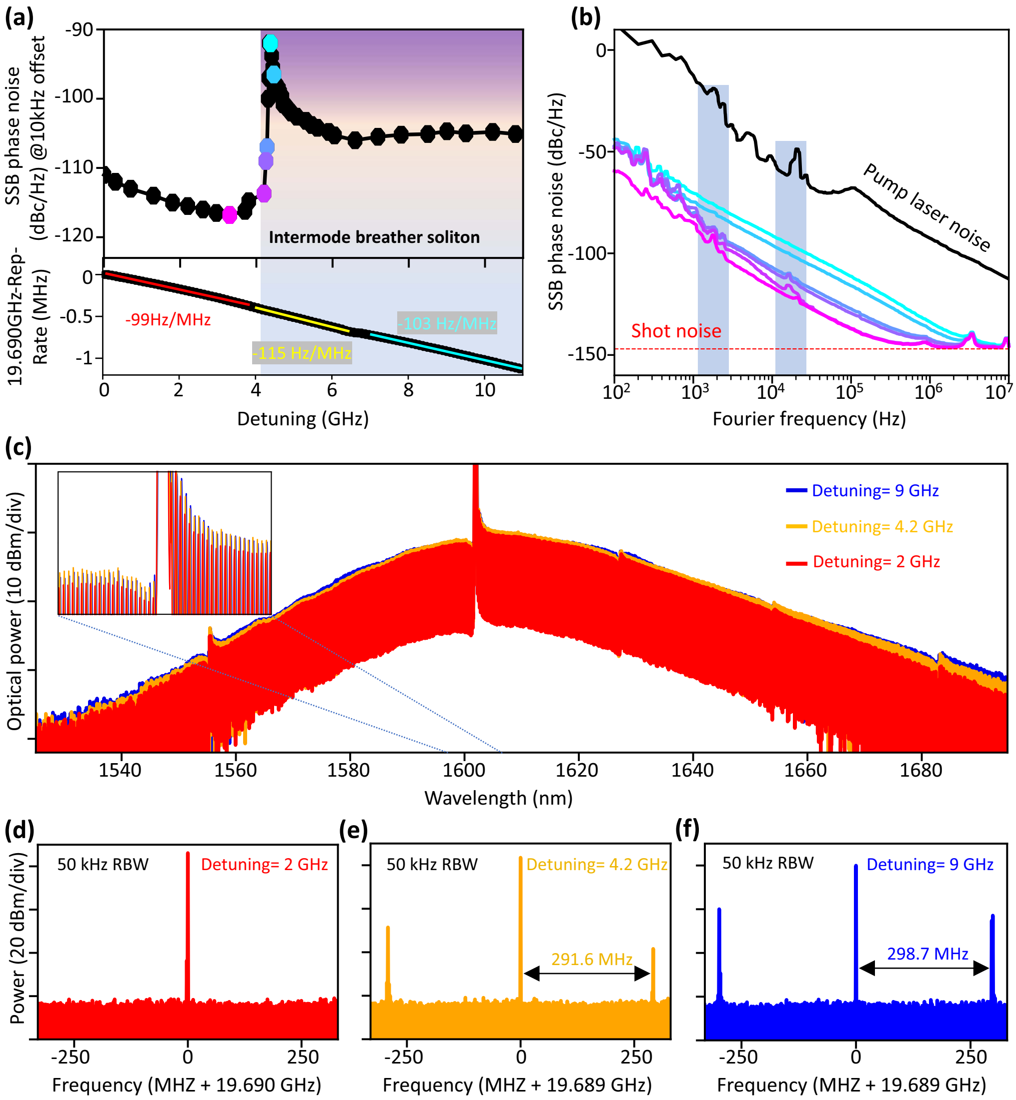

Fig. 3. Intermode breather solitons induced phase noise. (a) SSB phase noise of the 19.69 GHz signal at 10 kHz offset versus pump detuning with the repetition rate shift shown below. (b) SSB phase noise at different detuning frequencies [indicated by color in accordance with (a)]. (c) Optical spectrum at different detuning. Inset: spectrum near the pump showing absence of the soliton spectrum shift. (d)–(f) RF spectrum of the repetition rate with RBW of 50 kHz at three different detunings that match (c).

illustrates a comparison of microwave oscillators using a free-running chip-based microcomb.

The fractional frequency Allan deviation of our free-running microcomb is shown in Fig. 2(e). For short integration times, the Allan deviation is calculated by integrating the phase noise from Fig. 2(a); the result obtained from a frequency counter with a gate time of 10 ms [shown in Fig. 2(d)], without removing the linear drift, is used to compute the Allan deviation for longer integration times. The obtained Allan deviations for both cases show good overlap between the 10 ms and 1 s integration time, with a free-running Allan deviation at 8.1×10^{-9} in 1 s. Furthermore, the long-term stability of the free-running microcomb is dominated by the pump laser frequency fluctuations shown in the same figure.

C. Detuning Dependent Phase Noise Properties

We examine the phase noise of the microwave beat signal along the large soliton existence range to probe the possibility of degraded phase noise for different detuning. Figure 3(a) shows the 19.69 GHz SSB phase at 10 kHz offset for different detunings and the corresponding repetition rate shift. First, the monotonic linear behavior of the repetition rate frequency shift with respect to detuning demonstrates the absence of quiet point [31,41,55]. This also confirms that our low-noise operation does not manifest itself as a quiet-point operation. This is also experimentally verified by the absence of a significant soliton spectrum frequency shift with respect to our pump wavelength in Fig. 3(c). However, we still observe an increase of more than 20 dB in additional noise as we change the detuning. Such excess noise potentially originates from the formation of breather

Table 1. Phase Noise Performance Comparison of Low Repetition Rate Chip-Based DKS[a]

Ref.	Material	Rep-Rate (GHz)	$L(f)$ @ 10 kHz (dBc/Hz)	Coupling	Pump active control
Ref. [35]	Silica	22	−112	Tapered fiber	Pump-cavity detuning
Ref. [33]	Silica	21.9	−94	Tapered fiber	None
Ref. [32]	Silica	15.2	−111	Tapered fiber	Pump-cavity detuning
Ref. [40]	LN	19.8	−102	Integrated waveguide	None
Ref. [22]	SiN	19.6	−110	Integrated waveguide	Pump-cavity detuning
Ref. [36]	SiN	20.5	−80	Integrated waveguide	Pump-cavity detuning
Ref. [38]	SiN	10.8	−95	Integrated waveguide	Laser injection locking
Ref. [39]	SiN	20	−96	Integrated waveguide	Laser injection locking
Ref. [54]	SiN	25.25	−106	Integrated waveguide	None
Ref. [54]	SiN	25.25	−114	Integrated waveguide	Dual-pump RIN
This work	SiN	19.69	−117	Integrated waveguide	None

[a] All scaled to 19.69 GHz.

solitons due to AMX [56]. The amplitude modulation of the soliton increases the amplitude to phase noise conversion inside the microresonator, as shown in Fig. 3(b) where the pump frequency noise features at 2 kHz and 20 kHz offset (highlighted in the blue shaded regions) are now hidden (under the excess noise). Figures 3(d)–3(f) show the different RF spectra for different detunings before and after the aforementioned soliton breather formation, which starts at a detuning of ≈4.2 GHz, where the formation of sidebands on the microwave beat note of the soliton with a fundamental breathing frequency of ≈291.6 MHz starts to appear.

D. Repetition Rate Locking

We test whether the thermorefractive noise poses a fundamental limit when actively stabilizing the soliton repetition rate to an external reference, as shown in Fig. 4(a). We synthesize an ultralow phase noise 20 GHz microwave signal using a commercial self-referenced fiber frequency comb (FFC) system with a repetition rate of 250 MHz. One of the comb lines of the FFC is locked to an ultrastable laser with 1 Hz linewidth after subtraction of the carrier envelope offset frequency f_{ceo} to make the locking independent of f_{ceo} [57]. The low repetition rate of the FFC results in low power in the 80th harmonic of the repetition rate ($80 f_{\text{rep}}^{\text{FFC}} = 20$ GHz). Cascaded Mach–Zehnder fiber interferometers are used as interleavers for repetition rate multiplication to overcome this problem. This setup increases the signal level of the photodetected pulse train and reduces the amplitude-to-phase noise conversion in the photodetection [58]. An RF bandpass filter is used to select the 20 GHz microwave signal, and then amplified by a low-phase noise amplifier to 2 dBm. The synthesized 20 GHz phase noise is more than 10 dB lower than the TRN of our microresonator at 1 kHz offset. The 20 GHz microwave signal for the FFC is then mixed with the soliton microwave beat to generate a ≈310 MHz signal that is further mixed down to DC with a low-noise microwave generator (Rohde & Schwarz SMA100B) to generate the error signal. This error signal is fed to the PID controller that actuates the pump power using an intensity modulator (IM) before the microresonator. In our setup, the modulation of the pump power, rather than pump detuning, via ECDL current modulation provides a better lock-in sensitivity (see Appendix C). Figure 4(b) shows the phase noise of the stabilized soliton microwave beat, with SSB phase noise of −102 dBc/Hz at 100 Hz offset (instrument limited), −127 dBc/Hz at 1 kHz offset, and −136 dBc/Hz at 10 kHz offset. At 1 kHz the SSB phase noise is 14 dB lower than the optical-to-microwave divided TRN limit. This implies that one can overcome the TRN limit of SiN microresonators via active stabilization. Figure 4(c) shows the RF spectrum with 1 Hz RBW to demonstrate the long-term drift difference between the free-running and stabilized microwave beat notes. The stabilized soliton microwave beat note can track the frequency of the microwave signal $80 f_{\text{rep}}^{\text{FFC}}$ over a 25 kHz range before losing the servo lock, as shown in Fig. 4(d).

E. All-Optical Repetition Rate Locking

With the verified stabilization below the TRN bounds, we next stabilize the soliton microwave beat note using all-optical stabilization through the technique of two-point optical frequency division [59,60]. Figure 5(a) shows the experimental setup where the soliton spectrum is combined with the fiber comb spectrum, and then two optical lines of the soliton microcomb are selected using dense wavelength-division multiplexing (DWDM) filters. Each channel is sent into a photodiode to detect the beat between the soliton microcomb line and the fiber comb line. The two generated RF beat notes are mixed to generate a frequency that contains the relative noise between the two soliton microcomb lines. The resultant beat is mixed down to DC using an RF signal generator and sent into the servo controller. Figure 5(b) shows the three different optical channel spacings used in this measurement: 100 GHz, 400 GHz, and 1 THz. The corresponding stabilized phase noise for each of the three channel spacings is shown in Fig. 5(c), where the experimental improvement in each case follows the $20 \log_{10} f_{\text{spacing}}$. We note that the close-in phase noise, such as at 100 Hz, shows more than a 40 dB improvement, even below the microresonator TRN. Further phase noise reduction can be achieved by increasing the optical spacing of the two references. This demonstration verifies that the microwave-rate DKS microcombs can aid in two-point optical frequency division efforts, inheriting the stability of the two references to generate stable carrier signals below thermorefractive noise bounds.

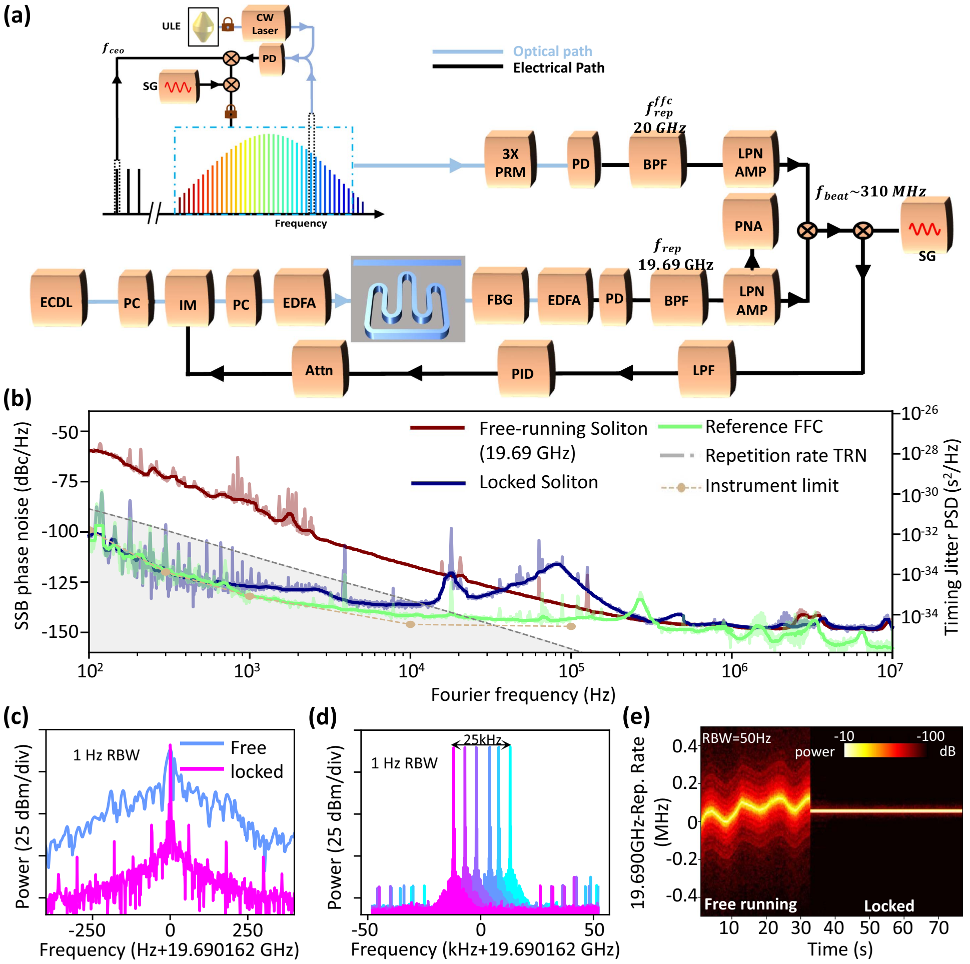

Fig. 4. Stabilized chip-scale optical frequency comb. (a) Stabilizing the repetition rate to an ultralow noise microwave signal synthesized using self-referenced fiber frequency combs. ULE, ultralow expansion cavity; PC, polarization controller; 3X PRM, three-stage pulse rate multiplier; ECDL, extended cavity laser diode; EDFA, erbium-doped fiber amplifier; SG, signal generator; FBG, fiber Bragg grating; PD, photodiode; RF BPF, RF bandpass filter; RF LPF, RF lowpass filter; LPN AMP, low-phase noise amplifier; Attn, attenuator; and PNA, phase noise analyzer. (b) SSB phase noise of the stabilized repetition rate (blue) shows active stabilization below the TRN limit (gray). The phase noise analyzer instrument limit is shown in light brown. (c) RF spectrum of the stabilized versus free-running repetition rate shown with 1 Hz RBW to examine the long-term frequency drift. (d) RF spectrum of the locked soliton repetition rate showing fine-tuning control of the repetition rate. The RBW is 1 Hz. (e) Example spectrogram of the repetition rate before and after locking.

3. CONCLUSION

In this work, we demonstrated a low repetition rate soliton based on a Si_3N_4 microresonator with a record low phase noise over a large pump detuning range without requiring active pump cavity detuning stabilization. The low-phase noise Si_3N_4 microresonator provides a compact and scalable solution for clean microwave signal generation. The measured free-running phase noise (scaled to 10 GHz) of −123 dBc/Hz at 10 kHz offset frequency is lower than that of existing chip-based dissipative Kerr soliton sources [22,32,33,35,36,39,40]. The low-noise performance was achieved with the assistance of an auxiliary mode and the minimal soliton spectrum shift yielding a −73 dB PM-to-PM noise conversion from laser noise to the soliton repetition rate. We have also observed AMX-induced spatiotemporal noise limiting the performance of our Si_3N_4 microresonator. Furthermore, we demonstrated that the fundamental thermorefractive noise of the soliton microwave signal can be suppressed by actively stabilizing our soliton to an ultrastable fiber frequency comb oscillator. The achieved phase noise of the stabilized soliton is 10 dB lower than the thermorefractive noise of the soliton. The use of an auxiliary mode with orthogonal polarization and a similar intensity profile increases the thermal correlation between the soliton mode and the dispersive wave mode, hence reducing the AMX-induced thermorefractive noise due to the difference in the intensity mode profile. Further delocalization of the mode with larger mode volumes and low confinement can lower the thermal noise of the microresonator frequency combs.

APPENDIX A: LINEAR CHARACTERIZATION OF THE MICRORESONATOR

Figure 6 shows the normalized transmission of the microresonator, where a strong TE–TM mode coupling occurs near 1602 nm as well as 1557 nm. A histogram of the loaded quality

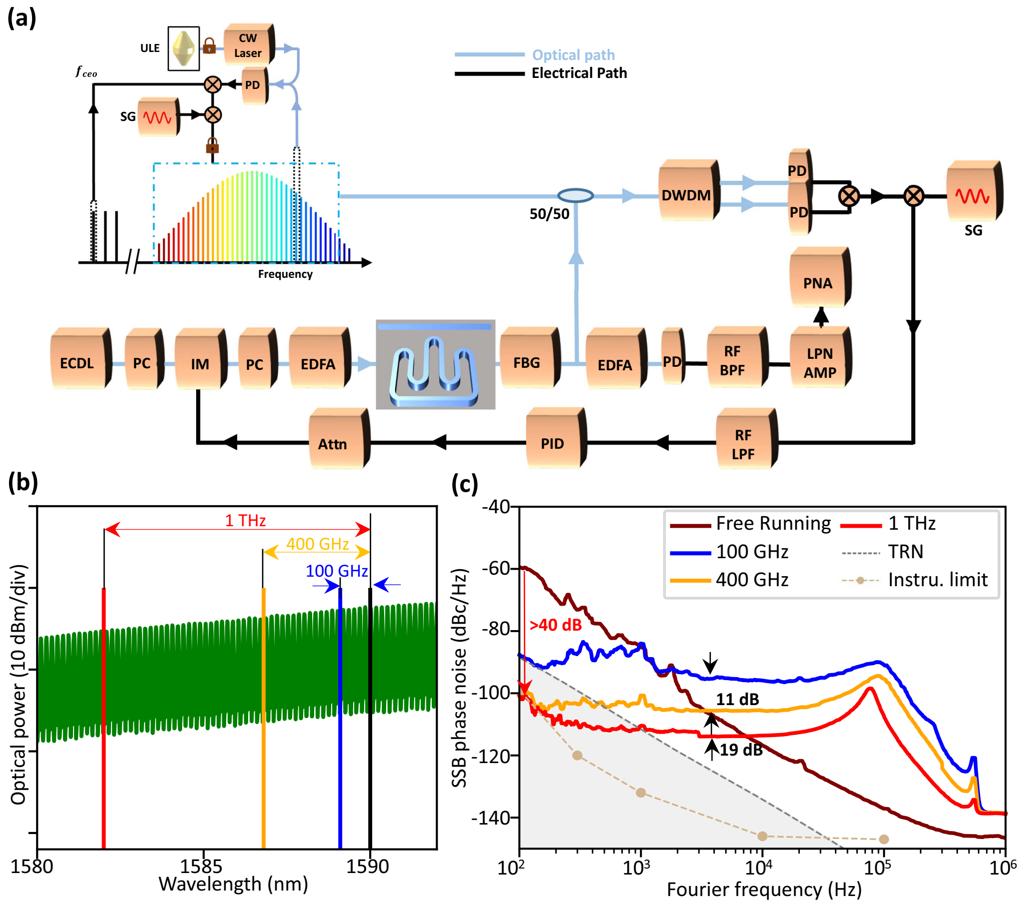

Fig. 5. Stabilization using optical frequency division (OFD). (a) Experimental setup. An optical coupler is used to couple the fiber comb with the microcomb. A dense WDM is used to filter out two frequency comb pairs. After each pair is photodetected, their beats are mixed. The resultant signal is down-mixed to DC and serves as the error signal. (b) Optical spectrum showing the separation between the comb pair. Three different frequency separations are illustrated as examples. (c) SSB phase noise of the locked repetition rate showing close to $20\log_{10}(N)$ division.

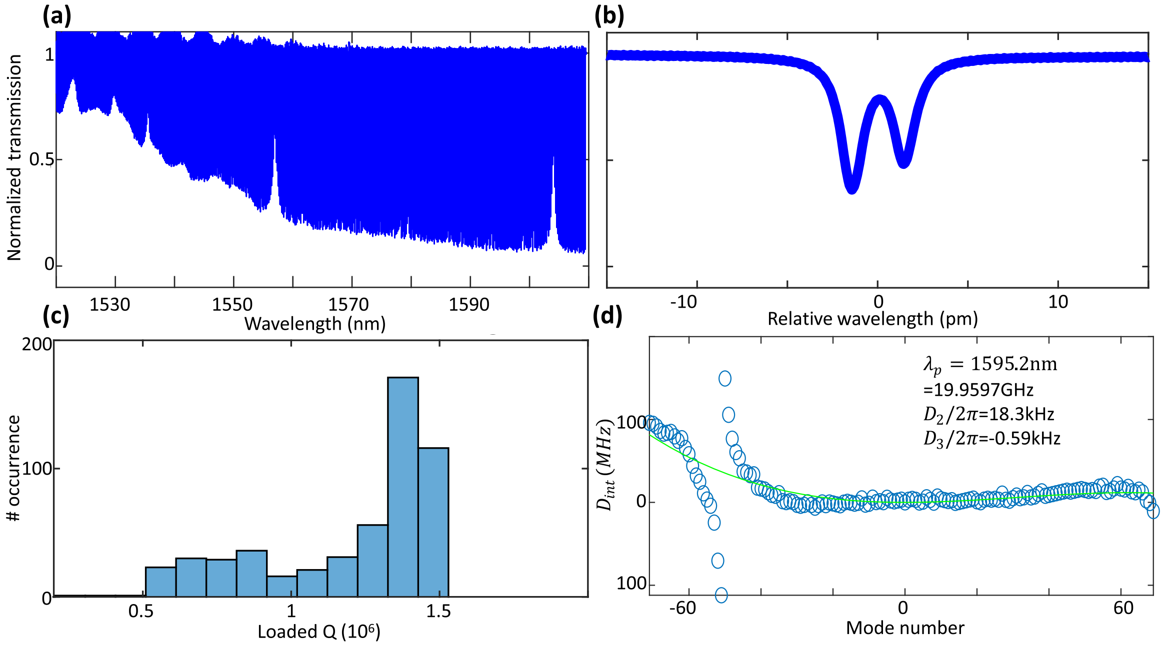

Fig. 6. Linear characterization of the microresonator. (a) Normalized transmission. (b) Hybridized TE–TM mode near 1603 nm. (c) Histogram of the loaded quality factor of the microresonator. (d) Integrated dispersion away from the avoided mode-crossing region.

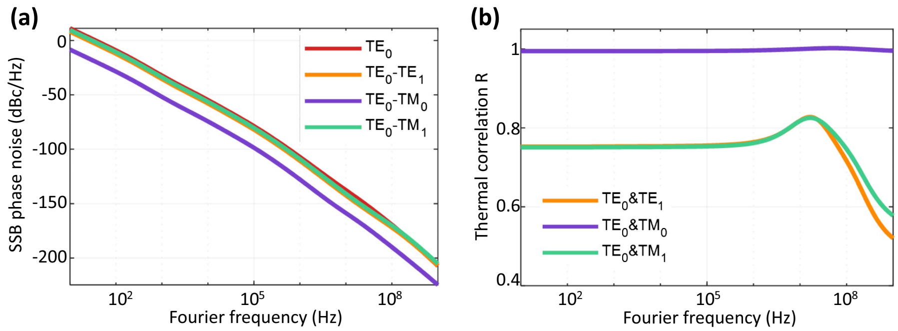

Fig. 7. Simulation of thermorefractive noise of the microresonator. (a) TRN of the soliton mode TE_0 and TRN of the differential mode of the soliton mode and other modes, taken at the frequency of the pump $f_p = 187$ THz. (b) Temperature correlation factor R between soliton mode and other different transverse modes.

factor of all TE mode resonances is shown in Fig. 6(c). The dispersion away from the avoided-mode crossing is slightly anomalous with D_2 of 18.3 kHz at 1595 nm and D_3 of −0.6 kHz.

APPENDIX B: THERMOREFRACTIVE NOISE

The thermorefractive noise (TRN) limit of the $\mathrm{Si_3N_4}$ resonator embedded in a $\mathrm{SiO_2}$ substrate is simulated based on the fluctuation-dissipation theorem as described in the literature [44,61,62]. Using FEM, we solve the thermal fluctuation of the microresonator $\delta\tilde{T}(\vec{r},\omega)$, using a heat transfer equation in the frequency domain,

$$i\omega\rho C_\nu \delta\tilde{T}(\vec{r},\omega) + \kappa\nabla^2\delta\tilde{T}(\vec{r},\omega) = i\omega T_0 \delta\tilde{S}(\vec{r},\omega), \qquad \textbf{(B1)}$$

where ρ is the material mass density, C_ν is the heat capacity, κ is the thermal conductivity, T_0 is the heat bath temperature, and $\tilde{S}$ is the fluctuation of the entropy. Here, a periodic entropy is used, which has the form $S = F_0 \cos(\omega t) q(\vec{r})$, where $q(\vec{r})$ is the normalized distribution of the electrical field intensity. The dissipated energy can then be calculated using $W_{\mathrm{diss}} = \int \frac{\pi\kappa}{\omega T_0} |\nabla\tilde{T}(\vec{r},\omega)|^2 \mathrm{d}^3\vec{r}$. The one-sided power spectral density of the frequency fluctuation of the resonator due to the refractive index fluctuations can be written as

$$S_{\mathrm{TRN}} = S_{\frac{\delta\omega}{\omega}} = \frac{2\hbar W_{\mathrm{diss}}}{\pi F_0^2} \coth\left(\frac{\hbar\omega}{2k_B T}\right). \qquad \textbf{(B2)}$$

The above formulation can be extended to calculate the thermal fluctuations due to the dispersive wave induced by avoided-mode crossing S_{AMX}, by taking $q_{12}(\vec{r}) = q_1(\vec{r}) - q_2(\vec{r})$, where q_{12} represents the difference between the normalized intensity profile of the two modes involved in the AMX process [32]. S_{AMX}, can also be expressed as

$$S_{\mathrm{AMX}} = S_{\mathrm{TRN1}} + S_{\mathrm{TRN2}} - 2R\sqrt{S_{\mathrm{TRN1}} S_{\mathrm{TRN2}}}, \qquad \textbf{(B3)}$$

where S_{TRN1} and S_{TRN2} are the thermorefractive noise of the soliton mode and the dispersive mode, respectively, and R is

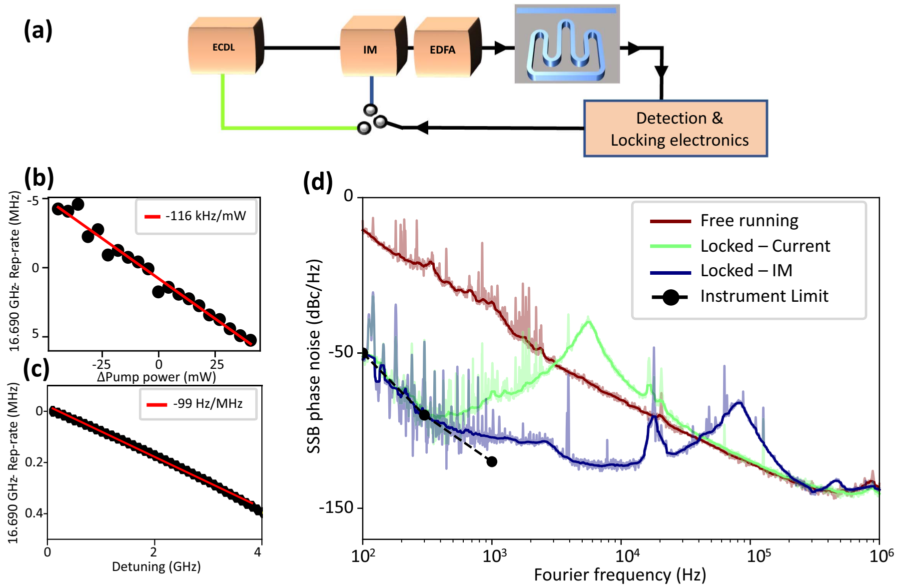

Fig. 8. Dependence of locking sensitivity on pump properties. (a) Locking setup, where an intensity modulator is used to actuate the pump power, and laser current to actuate the detuning. (b) The repetition rate as a function of the pump power change in the ring, was determined at −116 kHz/mW. (c) The repetition rate as a function of the pump frequency change, determined between −99 and −115 Hz/MHz. (d) Phase noise measurement of the locked repetition rate in the two cases. The laser current shows a smaller locking bandwidth due to insufficient sensitivity.

the thermal correlation between the two modes. The simulation results for the TRN of the soliton of the microresonator are illustrated in Fig. 7(a). Also, the TRN due to the soliton mode family and other modes is plotted on the same plot. Figure 7(b) shows the frequency-dependent thermal correlations between modes.

APPENDIX C: CHOICE OF THE ACTUATOR

Figure 8 shows the difference between locking using the laser current (detuning) or intensity modulator (power) where the sensitivity of each actuator with respect to the soliton repetition rate is shown in Figs. 8(b) and 8(c). The locking bandwidth using detuning is limited to 5 kHz due to a lack of sensitivity where higher loop gain is required. We choose to lock where a bandwidth of 100 kHz can be achieved.

Funding. Defense Advanced Research Projects Agency (HR001122C0017).

Acknowledgment. We acknowledge discussions with Tara Drake and Michele Giunta. We also acknowledge the loan of the Mach–Zender interleaver from Menlo Systems. A.A. acknowledges support from the Kuwait University scholarship program.

Author Contributions. A.A. conducted the experiments with assistance from H.C. and D.I.L. A.A. analyzed the data and performed the simulations. W.W. performed the device characterization. T.M. and A.C. contributed to the experiments. M.Y., G.-Q.L., and D.L.K. performed the device nanofabrication. A.A. and C.W.W. initiated the project. A.A. and C.W.W. wrote the manuscript.

Disclosures. The authors declare no conflicts of interest.

Data Availability. Data underlying the results presented in this paper are not publicly available at this time but may be obtained from the authors upon reasonable request.

REFERENCES

1. P. Del'Haye, A. Schliesser, O. Arcizet, *et al.*, "Optical frequency comb generation from a monolithic microresonator," Nature **450**, 1214–1217 (2007).
2. H. Liu, W. Wang, J. Yang, *et al.*, "Observation of deterministic double dissipative-Kerr-soliton generation with avoided mode crossing," Phys. Rev. Res. **5**, 013172 (2023).
3. A. L. Gaeta, M. Lipson, and T. J. Kippenberg, "Photonic-chip-based frequency combs," Nat. Photonics **13**, 158–169 (2019).
4. Y. Sun, J. Wu, M. Tan, *et al.*, "Applications of optical microcombs," Adv. Opt. Photon. **15**, 86 (2023).
5. J. Li, H. Lee, T. Chen, *et al.*, "Low-pump-power, low-phase-noise, and microwave to millimeter-wave repetition rate operation in microcombs," Phys. Rev. Lett. **109**, 233901 (2012).
6. T. E. Drake, T. C. Briles, J. R. Stone, *et al.*, "Terahertz-rate Kerr-microresonator optical clockwork," Phys. Rev. X **9**, 031023 (2019).
7. S.-W. Huang, J. Yang, M. Yu, *et al.*, "A broadband chip-scale optical frequency synthesizer at 2.7×10^{-16} relative uncertainty," Sci. Adv. **2**, e1501489 (2016).
8. J. Yang, S.-W. Huang, Z. Xie, *et al.*, "Coherent satellites in multispectral regenerative frequency microcombs," Commun. Phys. **3**, 27 (2020).
9. T. Fortier and E. Baumann, "20 years of developments in optical frequency comb technology and applications," Commun. Phys. **2**, 153 (2019).
10. X. Xie, R. Bouchand, D. Nicolodi, *et al.*, "Photonic microwave signals with zeptosecond-level absolute timing noise," Nat. Photonics **11**, 44–47 (2017).
11. E. C. Vargas, K. Şžafak, A. Dai, *et al.*, "Low noise photonic microwave oscillator based on a novel repetition rate stabilization," in *Joint Conference of the European Frequency and Time Forum and IEEE International Frequency Control Symposium (EFTF/IFCS)* (IEEE, 2023), pp. 1–2.
12. N. V. Nardelli, H. Leopardi, T. R. Schibli, *et al.*, "Optical and microwave metrology at the 10^{-18} level with an Er/Yb:glass frequency comb," Laser Photon. Rev. **17**, 2200650 (2023).
13. T. Udem, R. Holzwarth, and T. W. Hänsch, "Optical frequency metrology," Nature **416**, 233–237 (2002).
14. S.-W. Huang, H. Zhou, and J. Yang, , *et al.*, "Mode-locked ultrashort pulse generation from on-chip normal dispersion microresonators," Phys. Rev. Lett. **114**, 053901 (2015).
15. T. J. Kippenberg, A. L. Gaeta, M. Lipson, *et al.*, "Dissipative Kerr solitons in optical microresonators," Science **361**, eaan8083 (2018).
16. H. Guo, M. Karpov, E. Lucas, *et al.*, "Universal dynamics and deterministic switching of dissipative Kerr solitons in optical microresonators," Nat. Phys. **13**, 94–102 (2017).
17. Y. Li, S.-W. Huang, B. Li, *et al.*, "Real-time transition dynamics and stability of chip-scale dispersion-managed frequency microcombs," Light Sci. Appl. **9**, 52 (2020).
18. H. Zhou, Y. Geng, W. Cui, *et al.*, "Soliton bursts and deterministic dissipative Kerr soliton generation in auxiliary-assisted microcavities," Light Sci. Appl. **8**, 50 (2019).
19. B. Yao, S.-W. Huang, Y. Liu, *et al.*, "Gate-tunable frequency combs in graphene-nitride microresonators," Nature **558**, 410–414 (2018).
20. D. T. Spencer, T. Drake, T. C. Briles, *et al.*, "An optical-frequency synthesizer using integrated photonics," Nature **557**, 81–85 (2018).
21. W. Liang, D. Eliyahu, V. S. Ilchenko, *et al.*, "High spectral purity Kerr frequency comb radio frequency photonic oscillator," Nat. Commun. **6**, 7957 (2015).
22. J. Liu, E. Lucas, A. S. Raja, *et al.*, "Photonic microwave generation in the X- and K-band using integrated soliton microcombs," Nat. Photonics **14**, 486–491 (2020).
23. Y. Geng, H. Zhou, X. Han, *et al.*, "Coherent optical communications using coherence-cloned Kerr soliton microcombs," Nat. Commun. **13**, 1070 (2022).
24. M.-G. Suh and K. J. Vahala, "Soliton microcomb range measurement," Science **359**, 884–887 (2018).
25. Y.-S. Jang, H. Liu, J. Yang, *et al.*, "Nanometric precision distance metrology via hybrid spectrally resolved and homodyne interferometry in a single soliton frequency microcomb," Phys. Rev. Lett. **126**, 023903 (2021).
26. M.-G. Suh, X. Yi, Y.-H. Lai, *et al.*, "Searching for exoplanets using a microresonator astrocomb," Nat. Photonics **13**, 25–30 (2019).
27. P. J. Marchand, J. Riemensberger, J. C. Skehan, *et al.*, "Soliton microcomb based spectral domain optical coherence tomography," Nat. Commun. **12**, 427 (2021).
28. T. M. Fortier, M. S. Kirchner, F. Quinlan, *et al.*, "Generation of ultrastable microwaves via optical frequency division," Nat. Photonics **5**, 425–429 (2011).
29. S.-W. Huang, J. Yang, J. Lim, *et al.*, "A low-phase-noise 18 GHz Kerr frequency microcomb phase-locked over 65 THz," Sci. Rep. **5**, 13355 (2015).
30. W. Weng, E. Lucas, G. Lihachev, *et al.*, "Spectral purification of microwave signals with disciplined dissipative Kerr solitons," Phys. Rev. Lett. **122**, 013902 (2019).
31. E. Lucas, P. Brochard, R. Bouchand, *et al.*, "Ultralow-noise photonic microwave synthesis using a soliton microcomb-based transfer oscillator," Nat. Commun. **11**, 374 (2020).
32. Q.-F. Yang, Q.-X. Ji, L. Wu, *et al.*, "Dispersive-wave induced noise limits in miniature soliton microwave sources," Nat. Commun. **12**, 1442 (2021).
33. X. Yi, Q.-F. Yang, K. Y. Yang, *et al.*, "Soliton frequency comb at microwave rates in a high-*Q* silica microresonator," Optica **2**, 1078–1085 (2015).
34. D. Jeong, D. Kwon, I. Jeon, *et al.*, "Ultralow jitter silica microcomb," Optica **7**, 1108–1111 (2020).

35. D. Kwon, D. Jeong, I. Jeon, *et al.*, "Ultrastable microwave and soliton-pulse generation from fibre-photonic-stabilized microcombs," Nat. Commun. **13**, 381 (2022).
36. Z. Ye, F. Lei, K. Twayana, *et al.*, "Integrated, ultra-compact high-*Q* silicon nitride microresonators for low-repetition-rate soliton microcombs," Laser Photon. Rev. **16**, 2100147 (2022).
37. X. Ji, J. Liu, J. He, *et al.*, "Compact, spatial-mode-interaction-free, ultralow-loss, nonlinear photonic integrated circuits," Commun. Phys. **5**, 84 (2022).
38. W. Jin, Q.-F. Yang, L. Chang, *et al.*, "Hertz-linewidth semiconductor lasers using CMOS-ready ultra-high-*Q* microresonators," Nat. Photonics **15**, 346–353 (2021).
39. Q.-X. Ji, W. Jin, L. Wu, *et al.*, "Engineered zero-dispersion microcombs using CMOS-ready photonics," Optica **10**, 279–285 (2023).
40. Y. He, R. Lopez-Rios, U. A. Javid, *et al.*, "High-speed tunable microwave-rate soliton microcomb," Nat. Commun. **14**, 3467 (2023).
41. X. Yi, Q.-F. Yang, X. Zhang, *et al.*, "Single-mode dispersive waves and soliton microcomb dynamics," Nat. Commun. **8**, 14869 (2017).
42. F. Lei, Z. Ye, O. B. Helgason, *et al.*, "Optical linewidth of soliton microcombs," Nat. Commun. **13**, 3161 (2022).
43. A. B. Matsko and L. Maleki, "On timing jitter of mode locked Kerr frequency combs," Opt. Express **21**, 28862–28876 (2013).
44. G. Huang, E. Lucas, J. Liu, *et al.*, "Thermorefractive noise in silicon-nitride microresonators," Phys. Rev. A **99**, 061801 (2019).
45. A. Aldhafeeri, T. Yerebakan, Y.-S. Jang, *et al.*, "Frequency noise metrology of SiN microresonators with Qs of 100 million at the thermodynamical bounds," in *Conference on Lasers and Electro-Optics (CLEO)* (2023), paper SW4L.2.
46. M. Karpov, H. Guo, A. Kordts, *et al.*, "Raman self-frequency shift of dissipative Kerr solitons in an optical microresonator," Phys. Rev. Lett. **116**, 103902 (2016).
47. X. Yi, Q.-F. Yang, K. Y. Yang, *et al.*, "Theory and measurement of the soliton self-frequency shift and efficiency in optical microcavities," Opt. Lett. **41**, 3419–3422 (2016).
48. F. Lei, Z. Ye, and V. Torres-Company, "Thermal noise reduction in soliton microcombs via laser self-cooling," Opt. Lett. **47**, 513 (2022).
49. H. Weng, A. A. Afridi, J. Li, *et al.*, "Dual-mode microresonators as straightforward access to octave-spanning dissipative Kerr solitons," APL Photon. **7**, 066103 (2022).
50. J. R. Stone, T. C. Briles, T. E. Drake, *et al.*, "Thermal and nonlinear dissipative-soliton dynamics in Kerr-microresonator frequency combs," Phys. Rev. Lett. **121**, 063902 (2018).
51. W. Wang, H. Zhou, X. Jiang, *et al.*, "Polarization-diverse soliton transitions and deterministic switching dynamics in strongly-coupled and self-stabilized microresonator frequency combs," arXiv, arXiv:2303.03687 (2023).
52. R. Miao, K. Yin, C. Zhou, *et al.*, "Dual-microcomb generation via a monochromatically pumped dual-mode microresonator," Photon. Res. **12**, 163–171 (2024).
53. X. Xie, T. Sun, H. Peng, *et al.*, "Low-noise and broadband optical frequency comb generation based on an optoelectronic oscillator," Opt. Lett. **39**, 785–788 (2014).
54. R. Liu, C. Zhang, Y. Li, *et al.*, "Low-phase-noise microwave generation with a free-running dual-pumped Si_3N_4 soliton microcomb," Opt. Lett. **49**, 754–757 (2024).
55. E. Lucas, H. Guo, J. D. Jost, *et al.*, "Detuning-dependent properties and dispersion-induced instabilities of temporal dissipative Kerr solitons in optical microresonators," Phys. Rev. A **95**, 043822 (2017).
56. H. Guo, E. Lucas, M. H. Pfeiffer, *et al.*, "Intermode breather solitons in optical microresonators," Phys. Rev. X **7**, 041055 (2017).
57. J. Millo, M. Abgrall, M. Lours, *et al.*, "Ultralow noise microwave generation with fiber-based optical frequency comb and application to atomic fountain clock," Appl. Phys. Lett. **94**, 141105 (2009).
58. A. Haboucha, W. Zhang, T. Li, *et al.*, "Optical-fiber pulse rate multiplier for ultralow phase-noise signal generation," Opt. Lett. **36**, 3654–3656 (2011).
59. W. C. Swann, E. Baumann, F. R. Giorgetta, *et al.*, "Microwave generation with low residual phase noise from a femtosecond fiber laser with an intracavity electro-optic modulator," Opt. Express **19**, 24387–24395 (2011).
60. T. Tetsumoto, T. Nagatsuma, M. E. Fermann, *et al.*, "Optically referenced 300 GHz millimetre-wave oscillator," Nat. Photonics **15**, 516–522 (2021).
61. Y. Levin, "Fluctuation-dissipation theorem for thermo-refractive noise," Phys. Lett. A **372**, 1941–1944 (2008).
62. N. Kondratiev and M. Gorodetsky, "Thermorefractive noise in whispering gallery mode microresonators: analytical results and numerical simulation," Phys. Lett. A **382**, 2265–2268 (2018).